

CtxMIM: Context-Enhanced Masked Image Modeling for Remote Sensing Image Understanding

Mingming Zhang^{a,b}, Qingjie Liu^{a,b}, Yunhong Wang^{a,b}

^aState Key Laboratory of Virtual Reality Technology and Systems, Beihang University, Beijing, 100191, China

^bHangzhou Innovation Institute, Beihang University, Hangzhou, 310051, Zhejiang, China

Abstract

Learning representations through self-supervision on unlabeled data has proven highly effective for understanding diverse images. However, remote sensing images often have complex and densely populated scenes with multiple land objects and no clear foreground objects. This intrinsic property generates high object density, resulting in false positive pairs or missing contextual information in self-supervised learning. To address these problems, we propose a context-enhanced masked image modeling method (CtxMIM), a simple yet efficient MIM-based self-supervised learning for remote sensing image understanding. CtxMIM formulates original image patches as a reconstructive template and employs a Siamese framework to operate on two sets of image patches. A context-enhanced generative branch is introduced to provide contextual information through context consistency constraints in the reconstruction. With the simple and elegant design, CtxMIM encourages the pretraining model to learn object-level or pixel-level features on a large-scale dataset without specific temporal or geographical constraints. Finally, extensive experiments show that features learned by CtxMIM outperform fully supervised and state-of-the-art self-supervised learning methods on various downstream tasks, including land cover classification, semantic segmentation, object detection, and instance segmentation. These results demonstrate that CtxMIM learns impressive remote sensing representations with high generalization and transferability.

Keywords: Self-supervised learning, masked image modeling, Siamese, context consistency constraint, remote sensing

1. Introduction

Remote sensing images have been widely used in many applications, including precision agriculture, disaster management, city planning, and environment monitoring. With a growing number of satellites collecting remote sensing images ceaselessly, abundant remote sensing images are easy to access. However, annotations are technically challenging due to highly time-consuming and expertise knowledge than general benchmark datasets, *e.g.*, ImageNet (Russakovsky et al., 2015). Recently, self-supervised learning (SSL) has been increasingly emerging to pretrain models on extensive unlabeled data and demonstrated more robust performance than supervised learning on classification, segmentation, and detection. Therefore, the SSL paradigm has been receiving much attention from the remote sensing community and exploring

to obtain an efficient pretrained model on large-scale unlabeled data for remote sensing image understanding.

Existing advanced SSL methods (Manas et al., 2021; Ayush et al., 2021; Mall et al., 2023; Huang et al., 2024) primarily adopt contrastive learning (Chen et al., 2020b,a; Chen and He, 2021) for self-supervised remote sensing representation learning. Indeed, contrastive approaches learn representations invariant to season, geographical location, illumination, and viewing angle by employing extensive data augmentation, which have exceeded supervised learning-based methods. However, state-of-the-art contrastive methods typically require careful pretraining data organization in terms of temporal and geographical dimensions to prevent the pretraining collapse. Additionally, these methods generally concentrate on image-level feature learning by comparing two augmented views.



Figure 1: Object density gap between natural and remote sensing images. Natural images have apparent foreground objects in a relatively simple background, but remote sensing images contain multiple objects, especially no apparent foreground objects, in a vast and complicated scene. Hence, extending MIM to remote sensing images will miss contextual information during reconstruction due to considerably high object density.

Recently, SSL based on masked image modeling (MIM) has demonstrated potential performance in natural image representation learning (He et al., 2022a; Xie et al., 2022). These MIM methods reconstruct masked patches by randomly masking an image with a high masking ratio (*e.g.*, 75% in MAE (He et al., 2022a) and 80% in SimMIM (Xie et al., 2022)), which can learn good representations without extensive data augmentation. The pixel reconstruction idea of MIM is well-suited for remote sensing tasks since remote sensing analysis typically requires object-level or pixel-level features with fine-grained details rather than image-level features. However, applying MIM from natural images to remote sensing images still has limitations due to the considerably high object density in remote sensing images. Natural images have apparent foreground objects in a relatively simple background, *e.g.*, the cat, castle, and ambulance at the top of Figure 1, which can be easily repaired by inferring the whole from some parts through rich contextual information. Since remote sensing images are captured by sensors mounted on satellites, they generally contain multiple objects in a vast and complicated scene and typically have no apparent foreground objects, as illustrated at the bottom of Figure 1. Unlike natural images, some small land objects may be entirely masked by randomly masking, making pretraining convergence difficult, as demonstrated in ablation studies of subsection 4.6. Hence, MIM methods with a high masking ratio would hamper semantic extrapolating for remote sensing representation learning due to missing contextual information, as shown in Figure 2.

To address these issues, we propose a novel **C**ontext-enhanced **M**asked **I**mage **M**odeling

method (CtxMIM) to learn representations with high-level semantic and fine-grained details for remote sensing image analysis. CtxMIM first adopts a pixel reconstructive pre-text task to capture local information from the masked image. Then, a context-enhanced generative branch formulates the original patches as the reconstructive template, encouraging the reconstruction learning semantic extrapolating by providing meaningful contextual information. To train CtxMIM, a large-scale unlabeled dataset is collected, which contains over 1.28 million images without being carefully designed in terms of temporal and geographical dimensions.

We evaluate our approach on different tasks, including land cover classification, semantic segmentation, object detection, and instance segmentation. Following SOTA remote sensing SSL methods, we use EuroSAT (Helber et al., 2019), NWPU-RESISC45 (Cheng et al., 2017), DOTA (Xia et al., 2018), and SpaceNet (Van Etten et al., 2018) for comparison. Extensive experiments demonstrate that our method outperforms SOTA SSL methods and is more effective for remote sensing tasks than supervised learning on the common ImageNet (Russakovsky et al., 2015). In summary, our contributions are:

1. We propose a novel context-enhanced masked image modeling method (CtxMIM), a simple self-supervised learning framework to learn robust and transferable representations for efficient remote sensing image analysis.
2. CtxMIM is based on the analysis that remote sensing images have considerably higher object density than natural images. CtxMIM formulates the original image patches as the reconstructive template and introduces a context-enhanced generative branch to provide contextual information.
3. By pretraining on a large-scale unlabeled dataset, CtxMIM learns good representations to benefit image-level, object-level, and pixel-level downstream tasks. Moreover, we achieve state-of-the-art performance on land cover classification, semantic segmentation, object detection, and instance segmentation, demonstrating its transferability and superiority for remote sensing image analysis.

The remainder of this paper is organized as follows: Section 2 reviews related studies. Section 3

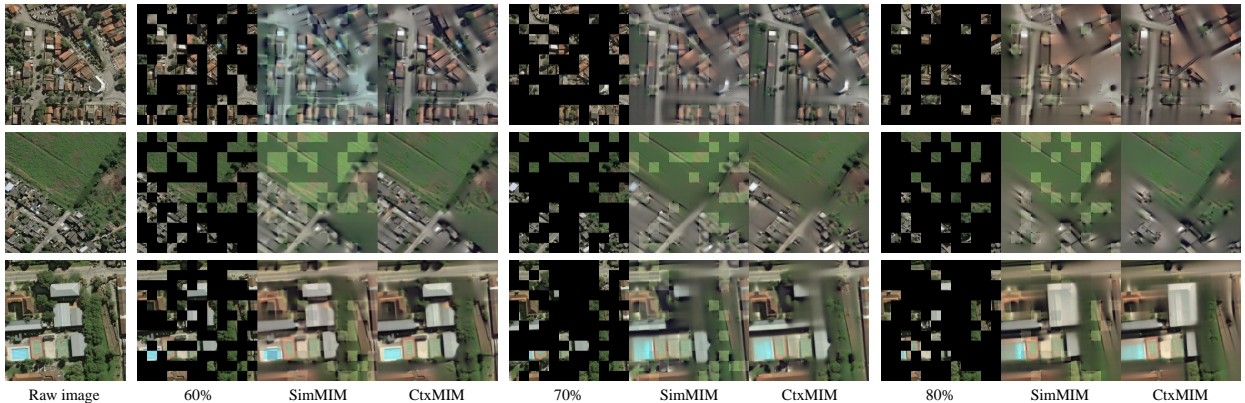


Figure 2: Reconstructive results on remote sensing images. The first column is raw images. The other triples show the masked image with different masking ratios (left), SimMIM (Xie et al., 2022) reconstruction (middle), and our CtxMIM reconstruction (right). SimMIM (Xie et al., 2022) and the proposed CtxMIM are pretrained on our collected dataset. Although more and more land objects are masked as the ratio becomes larger, our CtxMIM can still reconstruct masked images better in terms of texture and content.

introduces our proposed CtxMIM in detail. Section 4 first describes experimental settings, comparison methods, and evaluation metrics, then reports and discusses the experimental results quantitatively and qualitatively. Section 5 analyzes remote sensing pretraining in terms of model structure, performance, limitations, and future work. Section 6 concludes this work.

2. Related work

In this section, we first introduce two dominant self-supervised learning frameworks (*i.e.*, contrastive learning, and reconstructive learning) in the computer vision field. Motivated by increasing success in many computer vision tasks, self-supervised learning has been a prevalent paradigm for remote sensing pretraining, which is discussed in the following 2.3.

2.1. Contrastive Learning

Contrastive learning based methods (Oord et al., 2018; Tian et al., 2020) learn good representations by minimizing the distance between representations of positive pairs augmented from one image and pushing representations of negative pairs from different images away. SimCLR (Chen et al., 2020a) systematically analyzes the principles of contrastive learning methods and designs a simple framework for representation learning based on a Siamese network and extensive data augmentations. MoCos

(He et al., 2020; Chen et al., 2020b) introduce a dynamic large queue from different batches for contrastive learning and employ a moving-averaged encoder to maintain consistency. Since these methods require large batches or negative pairs to avoid collapsing, some methods (Grill et al., 2020; Caron et al., 2020; Chen and He, 2021; Zbontar et al., 2021; Li et al., 2021c) redesign the network structures, propose an innovative objective function, or introduce online clustering for representation learning. Recent contrastive methods (Kim and Song, 2021; Guo et al., 2022; Zhang et al., 2022; Reiss and Hoshen, 2023) have demonstrated superiority in different downstream tasks, even outperforming supervised learning. Although increasingly successful in many computer vision tasks, contrastive methods rely on extensive data augmentations and focus on image-level features, limiting the transferring performance in object-level or pixel-level cases.

2.2. Reconstructive Learning

Based on the idea of masked language modeling in NLP, reconstructive learning (Bao et al., 2021; He et al., 2022a; Xie et al., 2022; Wei et al., 2022; Liu et al., 2023b) learns representations through solving the reconstructive pre-text task. This line of work randomly masks a portion of image patches using a special [MASK] token and then predicts raw pixel values using masked image modeling. SimMIM (Xie et al., 2022) only uses a lightweight prediction head to reconstruct raw pixel values of

masked patches, facilitating good representation learning of the encoder. MAE (He et al., 2022a) first handles visible patches in the encoder, and then encoded patches and mask tokens are processed in the decoder, which can significantly reduce the computation overhead of the encoder. MixMAE (Liu et al., 2023a) reconstructs two original images from the mixed image by replacing the original masked patches with visible patches of another image, improving pretraining efficiency and consistency. With SOTA performance on various tasks, many related works have been studied, such as VideoMAE (Tong et al., 2022), MultiMAE (Bachmann et al., 2022), CIM (Fang et al., 2022), MSN (Assran et al., 2022), and SiamMAE (Gupta et al., 2024). However, these works have yet to be explored on large-scale remote sensing datasets.

2.3. Self-Supervised Learning in Remote Sensing

Recently, self-supervised learning has been broadly applied in remote sensing domains. For instance, many methods (Kang et al., 2020; Vincenzi et al., 2021; Li et al., 2021a; Stojnic and Risojevic, 2021; Jung et al., 2021) utilize contrastive learning to learn representations. SeCo (Manas et al., 2021) contrastively learns seasonal invariance by constructing a remote sensing dataset of different temporal information. Some methods (Ayush et al., 2021; Li et al., 2021b, 2022b) consider that geographical knowledge is the unique characteristic of remote sensing images, which can be used for contrastive learning. GeRSP (Huang et al., 2024) simultaneously learns representations with general and special knowledge from remote sensing and natural images by a teacher-student architecture. It designs self-supervised and supervised pretraining branches to generate the powerful pretrained model for remote sensing image understanding. Another attempt (Cong et al., 2022; He et al., 2023b; Mendieta et al., 2023; Hong et al., 2024) explores the masked image modeling paradigm for remote sensing feature pretraining by repairing masked images. SatMAE++ (Noman et al., 2024) leverages the scale information of remote sensing imagery to pretrain a transformer framework, finally achieving representations with more scales. ScaleMAE (Reed et al., 2023) reconsiders the scale information by explicitly learning relationships between data at different scales. After encoding a masked image, Scale-MAE reconstructs low/high frequency images at lower/higher scales. CrossScaleMAE (Tang et al., 2024), based on the Masked

Auto-Encoder (MAE), adopts scale augmentation techniques and introduces cross-scale consistency constraints to pretrain consistent and meaningful representations for downstream tasks. Besides, more relevant works have been studied for particular tasks, including change detection (Chen et al., 2023; de Gélis et al., 2023; Fang et al., 2023), land cover classification (Scheibenreif et al., 2022; Zeng and Geng, 2022; Bai et al., 2023; Xu et al., 2024), semantic segmentation (Li et al., 2022a; Muhtar et al., 2022; He et al., 2022b; Tang et al., 2023), and image fusion (He et al., 2023a; Sun et al., 2023; Wang et al., 2023).

While many methods have improved performance on different tasks, these methods are pretrained on datasets by carefully organizing in terms of temporal and geographical dimensions, leading to poor generalization ability. Since remote sensing images contain multiple interesting objects rather than one obvious foreground object in natural images, SSL methods remain challenging in the acquisition of positive pairs and reconstruction of masked image patches due to high object density. This work designs self-supervised learning based on reconstruction with a context-enhanced generative branch, which can learn representations with rich semantic and fine-grained details.

3. Method

In this section, We introduce the proposed CtxMIM, a novel MIM-based self-supervised learning for remote sensing image understanding. In the following, we will first describe the pretraining pipeline of the proposed CtxMIM. Then, we describe the main components of CtxMIM.

3.1. Overview

SSL, a prevalent paradigm in natural images, has been applied to large unlabeled remote sensing images and learned useful representations for downstream tasks (classification, segmentation, and detection). However, SSL in remote sensing still has been limited and lagged behind that in natural images since the object density is different between natural and remote sensing images. Natural images, such as the general benchmark dataset ImageNet (Russakovsky et al., 2015), are captured in daily scenes, and objects are mostly large in size. Hence, natural images typically have apparent foreground objects in a relatively simple background,

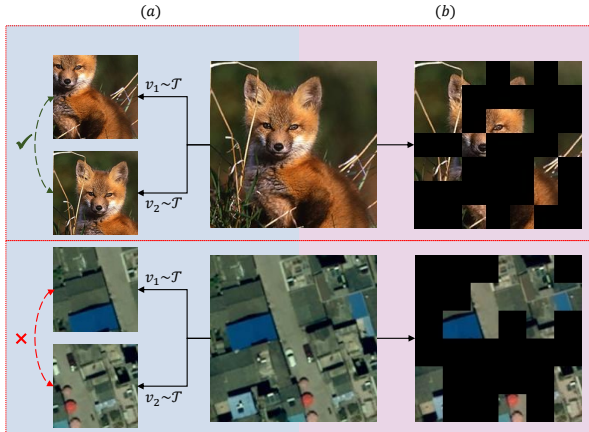


Figure 3: High object density in remote sensing images, resulting in mismatched positive pairs in contrastive learning or missing contextual information in reconstructive learning.

like the fox in Figure 3. Remote sensing images are captured by sensors mounted on satellites and contain multiple objects in a vast and complicated scene, especially no apparent foreground objects, as illustrated in the bottom of Figure 3. Therefore, the high object density poses challenges to the effectiveness of the SSL paradigm in remote sensing understanding, manifesting in the following issues: (1) Mismatched positive pairs when augmenting positive pairs from one image for contrastive learning, as shown in column (a) of Figure 3. (2) Missing contextual information caused by random masking strategies in reconstructive learning, as exemplified in column (b) of Figure 3.

To address this issue, we propose CtxMIM, a novel context-enhanced self-supervised representation learning method based on reconstructive learning. As shown in Figure 4, CtxMIM designs a reconstructive branch and a context-enhanced generative branch using an asymmetric Siamese network, which can learn representations by masked image modeling. For the reconstructive branch, CtxMIM first uniformly splits an input x into non-overlapping image patches x^p and then randomly mask x^p on patch-level to obtain a new input patches \hat{x}^p . Subsequently, CtxMIM takes as input \hat{x}^p to reconstruct the raw pixel values of the masked patches through the encoder-decoder architecture. The reconstructive branch is detailed in the subsection 3.2. Unlike natural images, the object density of remote sensing images is highly uneven, resulting in missing contextual information when randomly

masking image patches. To tackle this issue, we represent the original image patches as reconstructive templates rather than directly removing the masked patches. Based on this analysis, we introduce a context-enhanced generative branch to facilitate semantic reasoning by providing meaningful contextual information during the reconstruction.

Moreover, the context-enhanced generative branch shares the encoder and the decoder with the reconstructive branch, which is detailed in the subsection 3.3. For pretraining, we minimize the distance between raw pixel values x and the reconstructive values y for reconstructive and context-enhanced branches. Additionally, a context consistency loss is proposed to guide the reconstructive process of masked patches, which is described in subsection 3.4. Finally, our proposed CtxMIM is pretrained on a large-scale unlabeled dataset and learns impressive representations, which is beneficial for various downstream tasks (*e.g.*, *image-level*, *object-level*, and *pixel-level*).

3.2. Reconstruction of masked image patches

In the reconstruction stage, CtxMIM aims to learn local fine-grained features by restoring masked image patches. Given an input image $x \in \mathbb{R}^{C \times H \times W}$, CtxMIM firstly reshapes x to get image sequence patches $x^p \in \mathbb{R}^{N \times P^2 C}$, where H, W, C are the image height, width, and channel, respectively, P is the size of each image patch (*i.e.*, the height and width), and $N = (H/P) \cdot (W/P)$ is the number of image patches. Then, a patch-wise masking operation randomly masks some image patches, and a patch embedding operation encodes each image patch to get the new sequence input \hat{x}^p . Subsequently, an encoder f_θ takes the sequence input \hat{x}^p to extract latent representations \hat{h}^p , which are used in downstream tasks after pretraining. Finally, a decoder g_θ is used to reconstruct pixel values of masked patches \hat{y}^p on the latent representations. In our paper, we take Swin Transformer (Liu et al., 2021) as the feature encoder f_{swin} and a lightweight prediction head as the decoder g_{mlp} to output raw pixel values of the masked patches by following SimMIM (Xie et al., 2022), which can be formulated as:

$$\hat{y}^p = g_{mlp}(f_{swin}(\hat{x}^p) \odot \mathbb{I}_{\mathcal{M}}(\hat{x}_i^p)) \quad (1)$$

where $\mathbb{I}_{\mathcal{M}}(\cdot)$ is an indicator function that is 1 when each image patch \hat{x}_i^p is masked, 0 otherwise. \odot is an element-wise product operation.

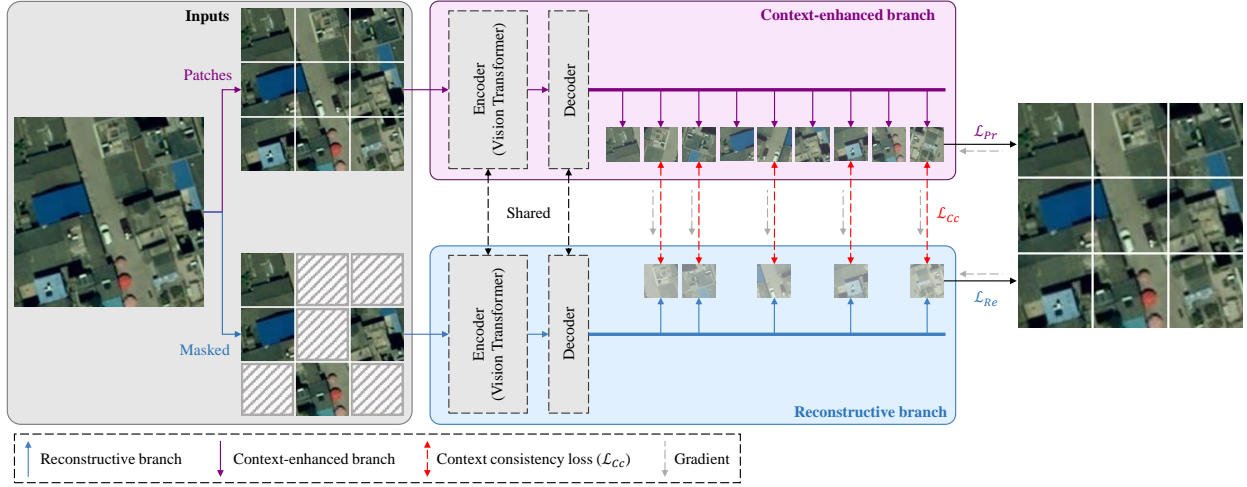


Figure 4: An illustration of CtxMIM, a simple yet efficient pretraining framework for remote sensing tasks. CtxMIM introduces a novel context-enhanced generative branch to provide contextual information by the context consistency constraint (\mathcal{L}_{Cc}) during the reconstruction, which formulates the original image patches as the reconstructive template. CtxMIM learns highly generalizable and transferable representations for various downstream tasks (e.g., image-level, object-level, and pixel-level).

3.3. Context-enhanced generative branch

Compared with natural images that are captured in daily scenes and objects are mostly with large size, remote sensing images typically cover multiple land objects with a large-scale and complex scene, which have no clear foreground objects. Therefore, some small land covers could be entirely masked, resulting in missing critical contextual information during the reconstruction. To tackle this issue, CtxMIM introduces a context-enhanced generative branch to provide contextual information. As illustrated in Figure 4, the context-enhanced generative branch inputs the image patches x^p to extract latent representations h^p with rich contextual information by the shared encoder f_θ . Then, the latent representations h^p are fed to the same decoder g_θ to predict the raw pixels y^p . The process of this branch is defined as follows:

$$y^p = g_{mlp}(f_{swin}(x^p) \odot \mathbb{I}_{\mathcal{M}}(x_i^p)) \quad (2)$$

where $\mathbb{I}_{\mathcal{M}}(\cdot)$ and \odot are the same operations as the reconstructive branch. Finally, the context-enhanced generative branch uses y^p as the template to make the reconstructive branch mimic feature extraction and learning semantic extrapolating by providing meaningful contextual information.

3.4. Training objective

CtxMIM first realizes a reconstructive learning objective by minimizing the distance between raw pixel values $x|_{\mathcal{M}}$ of the masked patches and the reconstructive values $y^{Re}|_{\mathcal{M}}$, which is calculated as:

$$\mathcal{L}_{Re} = \frac{\|y^{Re}|_{\mathcal{M}} - x|_{\mathcal{M}}\|}{N_M} \quad (3)$$

where N_M is the number of masked pixels. $\|\cdot\|$ is a distance function for calculating similarity between $y^{Re}|_{\mathcal{M}}$ and $x|_{\mathcal{M}}$. We adopt ℓ_1 loss for \mathcal{L}_{Re} calculation in our paper.

For the context-enhanced generative branch, CtxMIM learns contextual information by calculating the predicted loss \mathcal{L}_{Pr} between the predicted pixel values Y_{Pr} and raw pixel values X , which is similar to Equation 3. Then, a context consistency loss \mathcal{L}_{Cc} maximizes the similarity between $y^{Re}|_{\mathcal{M}}$ and the corresponding portion $y^{Pr}|_{\mathcal{M}}$, which is defined as:

$$\mathcal{L}_{Cc} = \text{Dist}(y^{Re}|_{\mathcal{M}} - y^{Pr}|_{\mathcal{M}}) \quad (4)$$

where $\text{Dist}(\cdot)$ is a similarity function to guide CtxMIM learning good contextual information. In our paper, we adopt ℓ_1 loss in the $\text{Dist}(\cdot)$ function. The context consistency loss \mathcal{L}_{Cc} mitigates pretraining convergence instability due to informational deficiencies.

Finally, the joint training objective of CtxMIM is calculated by the Equation 5:

$$\mathcal{L} = \mathcal{L}_{Re} + \mathcal{L}_{Pr} + \mathcal{L}_{Cc} \quad (5)$$

For \mathcal{L}_{Re} and \mathcal{L}_{Pr} , the gradients are propagated backward along their respective branches. As shown in Figure 4, the gradients from \mathcal{L}_{Cc} are propagated backward only to the reconstructive branch, prompting the encoder to mimic feature extraction and learning semantic extrapolating by providing meaningful contextual information. Additionally, it can also avoid trivial constant solutions by a stop-gradient operation. Finally, CtxMIM learns representations with rich semantic and local information by pretraining in a multi-task learning manner.

The proposed CtxMIM adopts Swin-B as the encoder and is implemented by the PyTorch framework. We use an AdamW optimizer with hyperparameters $\beta_1 = 0.9$, $\beta_2 = 0.999$, and $\epsilon = 1 \times 10^{-8}$, and the learning rate is set to 1×10^{-5} . The training lasts 200 epochs with 8 NVIDIA Tesla V100 GPUs. For pretraining, we collect a large-scale unlabeled remote sensing dataset captured from WorldView-3 using Google Earth Engine (Gorelick et al., 2017). This pretraining dataset is characterized by diverse topography and terrain, covering most regions (cities, villages, rivers, mountains, woodlands, and other terrain) of Asia.

4. Experiments

This section describes datasets and experiment settings for transfer learning. We evaluate our model on four downstream tasks and compare its performance with SOTA methods quantitatively and qualitatively. Finally, we conduct extensive ablation studies to verify the effectiveness of the proposed pretraining framework.

4.1. Experimental Settings

In downstream experiments, we select land cover classification, semantic segmentation, object detection, and instance segmentation, covering image-level, object-level, and pixel-level remote sensing tasks. To comprehensively confirm the performance of our method, we compare CtxMIM with supervised learning and SOTA self-supervised learning models, which are downloaded from their public websites. Finally, extensive experiments show that CtxMIM has strong performance on downstream tasks.

Sup. We employ three general backbones (ResNet-50 (He et al., 2016), ViT (Dosovitskiy et al., 2020), and Swin Transformer (Liu et al., 2021)) initialized with ImageNet pretraining for supervised learning comparison. In experiments, “Random Init.” and “ImageNet Pre.” denote that different backbones are initialized with random initialization and ImageNet pretraining, respectively. Besides, SatLas (Bastani et al., 2023) is compared as a remote sensing supervised method since it is pretrained on a large-scale remote sensing dataset with 137 categories under seven label types.

Self-Sup. For self-supervised learning comparison, we evaluate our approach with contrastive and reconstructive methods. We present additional details regarding the comparison methods in terms of datasets and experiment settings in the following:

1. **SeCo** (Manas et al., 2021), based on Momentum Contrast (MoCov2) (Chen et al., 2020b), pretrains a ResNet-50 backbone for 200 epochs with a batch size of 256. It collects a new dataset from Sentinel-2 (Drusch et al., 2012), designed to capture seasonal changes by sampling five images from distinct dates.
2. **Geo-Aware** (Ayush et al., 2021) pretrains a ResNet-50 backbone based on MoCov2 (Chen et al., 2020b) for 200 epochs with a batch size of 256. It creates GeoImageNet by extracting geo-coordinates for ImageNet (Rusakovsky et al., 2015). Finally, Geo-Aware uses the Functional Map of the World (fMoW) (Christie et al., 2018) and GeoImageNet for pretraining.
3. **CACo** (Mall et al., 2023) adopts the same pretraining settings and backbone as SeCo (Manas et al., 2021). CACo reconsiders the temporal signal to contrast images with long-term and short-term differences, spanning four years for the long-term and one year for the short-term.
4. **TOV** (Tao et al., 2023) is the original vision model with a ResNet50 backbone in the remote sensing field. By analyzing the influences of different data sampling and the selection of learning paths, it releases a benchmark dataset for pretraining. Finally, TOV is pretrained for 800 epochs with a batch size of 1024.
5. **CMID** (Muhtar et al., 2023) is a unified SSL framework which learns representations by combining the CL and MIM. CMID pretrains ResNet-50 and Swin-B backbones for

200 epochs on the MillionAID dataset with a batch size of 512 and 256, respectively.

6. **GeRSP** (Huang et al., 2024) is a MoCo-based framework using a teacher-student architecture. It pretrains a ResNet-50 backbone on the unlabeled Million-AID (MAID) (Long et al., 2021) and ImageNet (Russakovsky et al., 2015) for 200 epochs with a batch size of 128.
7. **ScaleMAE** (Reed et al., 2023) is based on the MAE architecture (He et al., 2022a), employing ViT-Large as the backbone. It uses the Functional Map of the World (FMoW) (Christie et al., 2018) RGB training set for 800 epochs with a batch size of 128.
8. **SatMAE++** (Noman et al., 2024) is a multi-scale pre-training approach, employing a Mask Autoencoder (MAE) framework. SatMAE++ pretrains a ViT-Large (Dosovitskiy et al., 2020) model on the Functional Map of the World (FMoW) (Christie et al., 2018) RGB training set. It lasts for 800 epochs with a batch size of 64.
9. **CrossScaleMAE** (Tang et al., 2024), based on Masked Auto-Encoder (MAE), pretrains a ViT-Large backbone on the Functional Map of the World (fMoW) (Christie et al., 2018) RGB training set. It is pretrained for 400 epochs with a batch size of 512.
10. **SpectralGPT** (Hong et al., 2024) is a foundation model by considering unique characteristics of spectral data in a MAE framework. It pretrains a ViT-Base backbone on an extensive dataset from the Sentinel2 satellite with over one million images. Finally, SpectralGPT is pretrained for 200 epochs with a batch size of 16.
11. **GFM** (Mendieta et al., 2023) collects a compact yet diverse dataset GeoPile from multiple sources to promote feature diversity. GFM introduces a multi-objective continual pretraining paradigm based on MIM (Xie et al., 2022), which can leverage the representations of ImageNet to learn valuable features. Finally, it pretrains a Swin-B backbone for 100 epochs with a batch size of 128.

4.2. Land Cover Classification

Implementation Details. We take two land cover classification datasets: (1) EuroSAT (Helber et al., 2019) is captured by the Sentinel-2 satellite over European cities. This dataset has 27,000

labeled images with a size of 64×64 . It contains 10 classes with 2,000-3,000 images per class. Following SeCo (Manas et al., 2021), we adopt the official train/val splits on EuroSAT. (2) NWPU-RESISC45 (Cheng et al., 2017) is a publicly available benchmark for remote sensing classification, which is published by Northwestern Polytechnical University (NWPU). The dataset contains 31,500 images with spatial resolutions ranging from 30 to 0.2m and a size of 256×256 . It covers 45 categories with 700 images in each category. Following GeRSP (Huang et al., 2024), we use the same train/val splits for this experiment.

For the land cover classification task, we initialize a backbone with different models and fine-tune a linear classifier head with ground truth labels in a supervised manner. We use an SGD optimizer with a learning rate of 1×10^{-4} , a momentum of 0.9, and a weight decay of 0.0005. All the models are trained for 100 epochs with a batch size of 64. During training, we adopt a linear-step policy with a decay ratio of 10 at 60% and 80% of the epochs. Finally, we report the top-1 accuracy for performance comparison.

Quantitative Results. Table 1 shows the top-1 accuracy of different methods on two datasets using fully supervised and self-supervised learning. For the EuroSAT dataset, we can see that CtxMIM outperforms the ImageNet supervised Swin-B backbone by +5.49%, illustrating that SSL on a large-scale remote sensing dataset improves performance for remote sensing downstream tasks. Additionally, CtxMIM achieves +6.15% higher top-1 accuracy than reconstructive learning methods, demonstrating that our approach learns robust and good transferable remote sensing representations for the land cover classification task. For the NWPU-RESISC45 dataset, we observe that CtxMIM improves the model of the Swin-B backbone initialized with the ImageNet supervised pretraining by +4.4% higher, proving that the domain gap exists between natural and remote sensing images. We find that CtxMIM outperforms contrastive and reconstructive pretraining methods by +2.37% and +1.97% higher, respectively.

4.3. Semantic Segmentation

Implementation Details. We use the SpaceNet (Rio) dataset (Van Etten et al., 2018) for the semantic segmentation task. This dataset contains 6,940 satellite images with binary building masks. We fine-tune a PSANet (Zhao et al., 2018) with the

Table 1: Top-1 accuracy on EuroSAT and NWPU-RESISC45 for land cover classification. CtxMIM obtains the best performance.

	Method	Backbone	EuroSAT Top-1 Acc. \uparrow	NWPU-RESISC45 Top-1 Acc. \uparrow
Sup.	Random Init.	ResNet50	77.74	45.88
	ImageNet Pre.	ResNet50	98.38	93.88
	ImageNet Pre.	ViT-B	89.83	82.68
	ImageNet Pre.	ViT-L	89.94	84.36
	ImageNet Pre.	Swin-B	93.38	90.80
	SatLas (Bastani et al., 2023)	ResNet50	96.62	86.23
	SatLas (Bastani et al., 2023)	Swin-B	83.44	79.88
Self-Sup.	SeCo (Manas et al., 2021)	ResNet50	95.09	61.52
	Geo-Aware (Ayush et al., 2021)	ResNet50	95.66	81.15
	CACo (Mall et al., 2023)	ResNet50	96.59	68.60
	TOV (Tao et al., 2023)	ResNet50	57.81	46.74
	CMID (Muhtar et al., 2023)	ResNet50	91.07	76.07
	GeRSP (Huang et al., 2024)	ResNet50	98.29	92.83
	ScaleMAE (Reed et al., 2023)	ViT-L	86.12	78.04
	SatMAE++ (Noman et al., 2024)	ViT-L	87.83	82.60
	CrossScaleMAE (Tang et al., 2024)	ViT-L	72.81	84.76
	SpectralGPT (Hong et al., 2024)	ViT-B	84.61	71.04
	GFM (Mendieta et al., 2023)	Swin-B	88.87	84.42
	CMID (Muhtar et al., 2023)	Swin-B	92.72	93.23
	CtxMIM (ours)	Swin-B	98.87	95.20

Table 2: Mean intersection over union (mIoU) and mean accuracy (mAcc) on SpaceNet (Rio) semantic segmentation task. Our method consistently improves supervised and self-supervised learning by large margins.

	Method	Backbone	mIoU \uparrow	mAcc \uparrow
Sup.	Random Init.	ResNet50	72.24	80.20
	ImageNet Pre.	ResNet50	75.70	83.98
	ImageNet Pre.	ViT-B	75.47	83.78
	ImageNet Pre.	ViT-L	76.34	84.34
	ImageNet Pre.	Swin-B	72.56	81.21
	SatLas (Bastani et al., 2023)	ResNet50	74.56	82.38
	SatLas (Bastani et al., 2023)	Swin-B	67.86	76.22
Self-Sup.	SeCo (Manas et al., 2021)	ResNet50	73.89	81.63
	Geo-Aware (Ayush et al., 2021)	ResNet50	74.99	82.30
	CACo (Mall et al., 2023)	ResNet50	74.98	82.77
	TOV (Tao et al., 2023)	ResNet50	74.12	81.89
	CMID (Muhtar et al., 2023)	ResNet50	71.53	79.28
	GeRSP (Huang et al., 2024)	ResNet50	76.29	84.47
	ScaleMAE (Reed et al., 2023)	ViT-L	77.21	85.12
	SatMAE++ (Noman et al., 2024)	ViT-L	77.25	85.40
	CrossScaleMAE (Tang et al., 2024)	ViT-L	75.55	83.87
	SpectralGPT (Hong et al., 2024)	ViT-B	69.17	77.78
	GFM (Mendieta et al., 2023)	Swin-B	72.81	81.71
	CMID (Muhtar et al., 2023)	Swin-B	65.98	73.72
	CtxMIM (ours)	Swin-B	79.22	87.20

Table 3: Average precision (AP) and average recall (AR) under different intersection over union thresholds on DOTA object detection task. $F1/F1_{75}$ calculated by AP/AP_{75} and AR/AR_{75} measures the performance more comprehensively/accurately.

Method	Backbone	AP	AP_{50}	AP_{75}	AP_s	AP_m	AP_l	AR	AR_{50}	AR_{75}	AR_s	AR_m	AR_l	$F1$	$F1_{75}$
Random Init.	ResNet50	24.2	43.9	25.0	13.4	25.7	27.5	40.1	70.8	40.9	22.7	43.8	52.5	30.2	31.0
ImageNet Pre.	ResNet50	35.9	61.3	38.1	21.2	37.2	45.6	46.7	75.2	50.4	29.1	50.2	59.5	40.6	43.4
ImageNet Pre.	Swin-B	36.4	64.3	37.8	23.3	38.9	44.1	48.7	81.9	51.8	32.2	53.6	59.4	41.7	43.7
SatLas (Bastani et al., 2023)	ResNet50	30.0	52.8	31.5	15.8	30.7	38.7	41.1	69.4	43.7	22.9	44.0	54.0	34.7	36.6
SatLas (Bastani et al., 2023)	Swin-B	27.8	50.7	28.7	18.0	28.6	34.0	42.5	75.1	43.8	27.7	46.9	52.7	33.6	34.7
SeCo (Manas et al., 2021)	ResNet50	32.0	55.4	33.9	18.6	32.7	38.5	44.7	74.7	47.6	28.0	48.1	55.1	37.3	39.6
Geo-Aware (Ayush et al., 2021)	ResNet50	33.2	58.0	34.3	17.8	34.4	41.9	44.5	73.9	47.4	26.7	47.9	56.1	38.0	39.8
CACo (Mall et al., 2023)	ResNet50	33.7	58.5	35.4	19.9	34.6	41.4	45.7	75.5	48.5	28.8	48.8	56.8	38.8	40.9
TOV (Tao et al., 2023)	ResNet50	35.2	61.7	36.6	21.6	36.2	44.2	46.4	76.8	49.3	30.1	49.3	58.5	40.0	42.0
CMID (Muhtar et al., 2023)	ResNet50	36.3	63.0	38.3	21.1	38.0	44.8	48.1	79.9	51.8	28.8	52.9	60.0	41.4	44.0
GeRSP (Huang et al., 2024)	ResNet50	37.6	63.3	39.4	22.0	38.6	47.3	47.9	76.0	51.9	29.8	51.4	60.2	42.1	44.8
GFM (Mendieta et al., 2023)	Swin-B	35.4	62.7	36.8	22.5	38.0	44.1	48.8	81.4	52.1	32.0	53.5	60.1	41.0	43.1
CMID (Muhtar et al., 2023)	Swin-B	27.3	51.0	27.5	17.2	28.7	32.6	42.2	75.9	43.1	26.4	47.0	52.0	33.2	33.6
CtxMIM (ours)	Swin-B	37.9	62.8	40.9	22.9	38.6	48.8	49.9	78.6	54.3	31.9	53.8	62.8	43.1	46.7

pretrained Swin-B backbone by CtxMIM. We use an AdamW optimizer with a batch size of 8 and a learning rate of 1×10^{-4} . We report mean intersection over union (mIoU) and mean accuracy (mAcc) to compare CtxMIM with comparison methods.

Quantitative Results. Table 2 presents mIoU and mAcc values of different methods on SpaceNet (Rio). The results show that our method achieves more considerable performance gains by +6.66% and +5.99% for supervised learning from the ImageNet pretrained weight with a Swin-B backbone. Compared with self-supervised learning, our method improves the mIoU performance by +2.93% and +1.97% over SOTA contrastive and reconstructive learning methods. Consistent experimental results demonstrate the effectiveness of our method for the semantic segmentation task.

4.4. Object Detection

Implementation Details. We use the DOTA dataset (Xia et al., 2018) to verify the object detection performance. DOTA dataset consists of 2,806 high-resolution satellite images with sizes ranging from 800×800 to $4,000 \times 4,000$. This dataset has 15 different categories with bounding box annotations and is split into 800×800 following GeRSP (Huang et al., 2024). Then, we fine-tune a RetinaNet (Lin et al., 2017) with an AdamW optimizer, a batch size of 4, a learning rate of 1×10^{-5} , and a weight decay of 0.05. We use the standard MS-COCO metrics (Lin et al., 2014), including average precision (AP) and average recall (AR) under different intersection over union thresholds, to compare CtxMIM with supervised and self-supervised methods on this task. Moreover, we calculate $F1$ and $F1_{75}$ to evaluate CtxMIM more comprehensively and accurately.

Quantitative Results. Table 3 reports results from comprehensive experiments on the DOTA dataset compared with supervised and self-supervised learning methods. CtxMIM consistently obtains the best performance across supervised and self-supervised learning methods. Specifically, CtxMIM gains +1.4% and +3% improvements on $F1$ and $F1_{75}$ over ImageNet supervised learning with a Swin-B backbone. Furthermore, CtxMIM improves the indicator $F1$ by +1% and 2.1% compared with contrastive and reconstructive learning methods. The extraordinary performance demonstrates that CtxMIM learns impressive representations for the object detection task.

4.5. Instance Segmentation

Implementation Details. SpaceNet (LasVegas) dataset (Van Etten et al., 2018) is used for instance segmentation task, consisting of 3,851 images across Las Vegas collected from WorldView-3 satellites. The size of images is 650×650 with a spatial resolution of 30 cm/pixel. The dataset contains 151,367 building polygon footprints in GeoJSON format. In our experiment, this dataset is randomly divided into train/test/validation subsets with a ratio of 8:1:1. We fine-tune MaskRCNN (He et al., 2017) with the ed Swin-B backbone from our CtxMIM on SpaceNet (LasVegas), using an AdamW optimizer, a learning rate of 0.0001, a batch size of 4. Finally, we report AP^m , AP_{50}^m , and AP_{75}^m under different intersections over union thresholds in the segmentation level.

Quantitative Results. As shown in Table 4, our approach learns transferable representations, outperforming all the comparison methods. Compared with supervised learning, CtxMIM improves the ImageNet supervised pretraining by +1.7% AP^m

Table 4: AP^m , AP_{50}^m , and AP_{75}^m on SpaceNet (Las Vegas) instance segmentation task. CtxMIM outperforms comparison methods (+2.2% and +1.1% on AP_{75}^m for Sup. and Self-Sup., respectively).

	Method	Backbone	AP^m	AP_{50}^m	AP_{75}^m
Sup.	Random Init.	ResNet50	16.3	34.8	13.1
	ImageNet Pre.	ResNet50	51.0	82.6	60.3
	ImageNet Pre.	ViT-B	58.4	88.1	69.7
	ImageNet Pre.	ViT-L	58.8	88.2	70.7
	ImageNet Pre.	Swin-B	45.6	78.4	50.8
	SatLas (Bastani et al., 2023)	ResNet50	39.3	73.4	39.3
	SatLas (Bastani et al., 2023)	Swin-B	29.8	59.2	27.3
Self-Sup.	SeCo (Manas et al., 2021)	ResNet50	40.8	73.7	42.4
	Geo-Aware (Ayush et al., 2021)	ResNet50	48.9	80.9	56.3
	CACo (Mall et al., 2023)	ResNet50	44.9	77.8	49.4
	TOV (Tao et al., 2023)	ResNet50	41.5	74.2	43.8
	CMID (Muhtar et al., 2023)	ResNet50	42.9	74.1	47.8
	GeRSP (Huang et al., 2024)	ResNet50	54.3	85.1	65.4
	ScaleMAE (Reed et al., 2023)	ViT-L	60.0	89.4	71.8
	SatMAE++ (Noman et al., 2024)	ViT-L	59.4	89.0	71.7
	CrossScaleMAE (Tang et al., 2024)	ViT-L	58.3	87.5	70.0
	SpectralGPT (Hong et al., 2024)	ViT-B	57.9	88.0	69.2
	GFM (Mendieta et al., 2023)	Swin-B	47.2	80.0	53.5
	CMID (Muhtar et al., 2023)	Swin-B	32.7	63.6	31.3
	CtxMIM (ours)	Swin-B	60.5	87.8	72.9

Table 5: Ablation study. LcC, SS, OD, and IS denote land cover classification, semantic segmentation, object detection, and instance segmentation, respectively. ‘- C-E’ removes the context-enhanced generative branch from CtxMIM.

Method	LcC (Acc.)	SS (mIoU)	OD ($F1_{75}$)	IS (AP^m)
CtxMIM	98.87	79.22	46.70	60.50
- C-E	96.90	76.91	44.0	59.10

and +2.2% AP_{75}^m , respectively. Moreover, CtxMIM achieves +0.5% AP^m and +1.1% AP_{75}^m higher compared with the SOTA self-supervised learning method ScaleMAE (Reed et al., 2023). The impressive results illustrate that CtxMIM learns good representations with high-level semantic and fine-grained details.

4.6. Ablation Study

We conduct ablation studies to verify the effectiveness of the designed context-enhanced generative branch on four typical remote sensing tasks, respectively. We adopt general datasets and critical indicators to measure performance, including EuroSAT (Helber et al., 2019), SpaceNet (Rio) (Van Etten et al., 2018), DOTA (Xia et al.,

2018), and SpaceNet (LasVegas) (Van Etten et al., 2018). As reported in Table 5, CtxMIM outperforms CtxMIM without the context-enhanced generative branch by +1.97% on top-1 accuracy, 2.31% on mIoU, +2.7% on $F1_{75}$, and +1.4% on AP^m . The consistent improvements have confirmed that the context-enhanced generative branch can significantly improve the performance, illustrating its superiority.

Additionally, Figures 5 and 6 show some CtxMIM reconstructive samples on various datasets with different masking ratios 70%, 75%, 80%, and 85%. The qualitative results demonstrate CtxMIM’s proficiency in recovering high-quality masked patches, particularly at higher masking ratios. This observation demonstrates its ability to acquire robust features for remote sensing image analysis.

5. Discussion

In this section, we further analyze our method in terms of model structure and performance and then discuss limitations and future work about SSL in remote sensing.

Model scalability. SSL methods in remote sensing employ contrastive learning to pretrain foun-

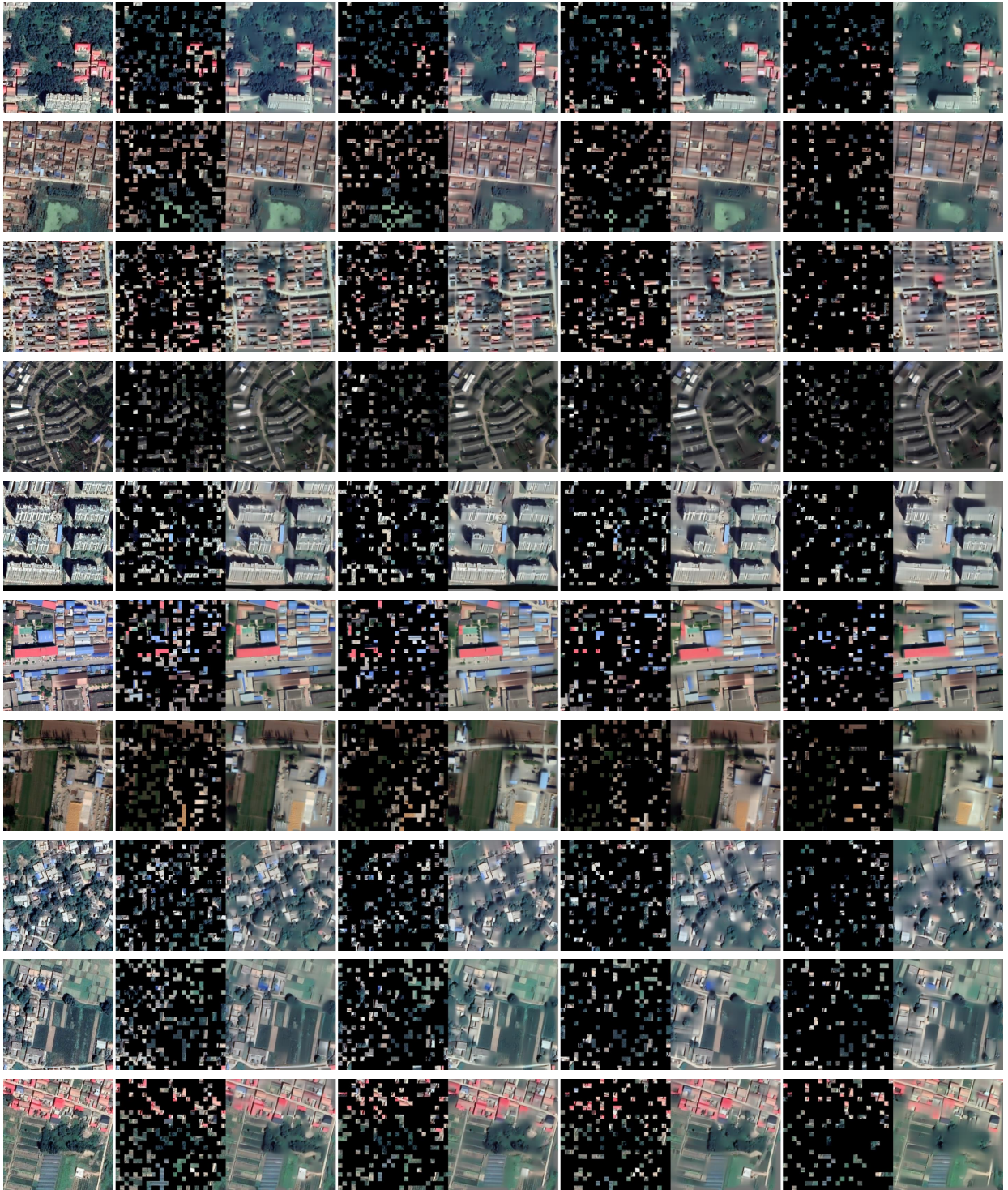


Figure 5: Some CtxMIM reconstructive samples on our pretraining dataset. Each row shows the ground truth, four 2-tuples (the masked image and the CtxMIM reconstruction) of different masking ratios 70%, 75%, 80%, and 85% from left to right.

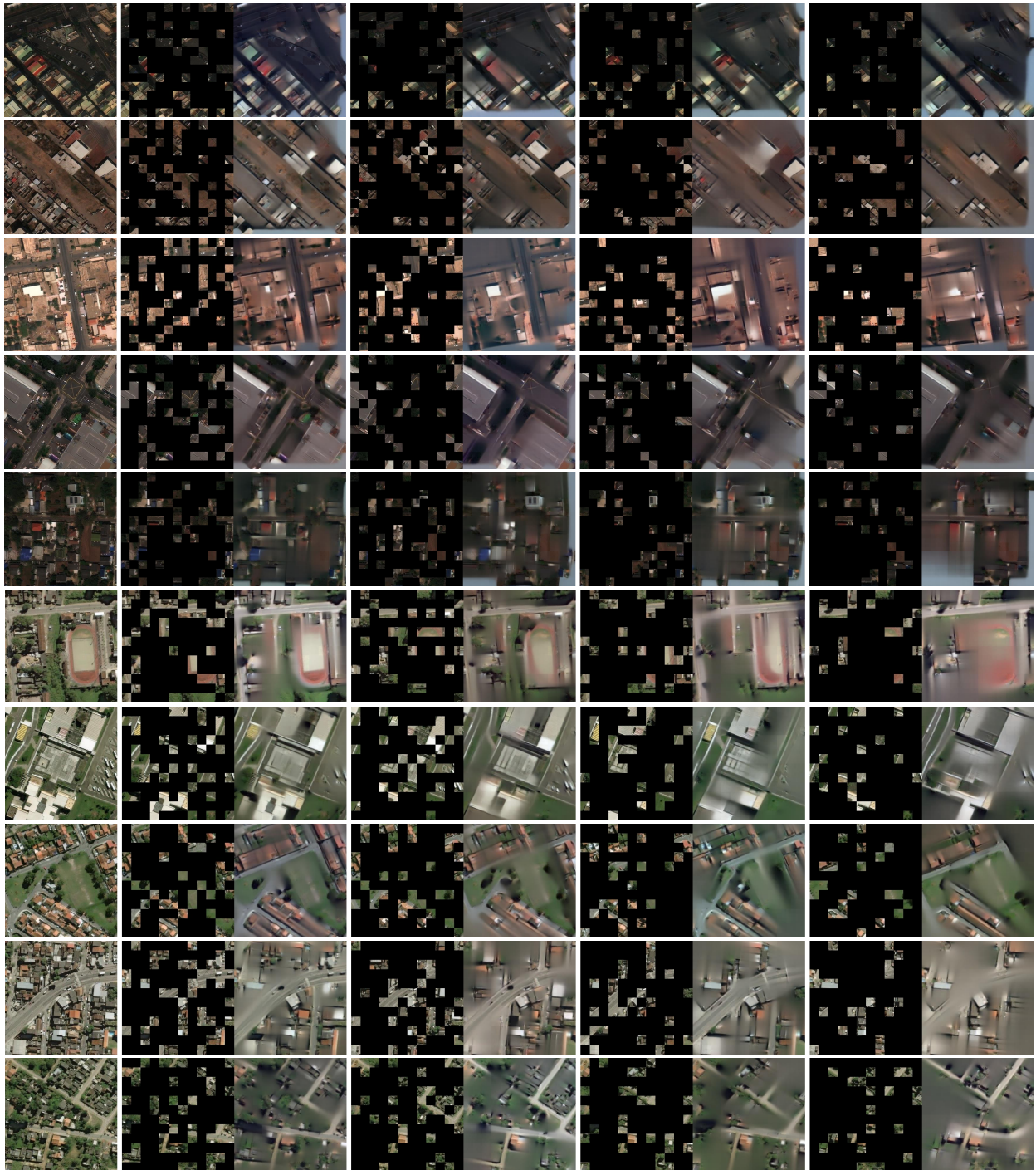


Figure 6: Some CtxMIM reconstructive samples on xView (Lam et al., 2018) and SpaceNet (Van Etten et al., 2018). Each row shows the ground truth, four 2-tuples (the masked image and the CtxMIM reconstruction) of different masking ratios 70%, 75%, 80%, and 85% from left to right.

dation models and have demonstrated higher performance on different remote sensing tasks. For extensive data augmentations, these methods consider intrinsic characteristics of remote sensing images to obtain contrastive pairs, like SeCo (Manas et al., 2021), CACo (Mall et al., 2023), and SatMAE (Cong et al., 2022) leveraging the temporal information, and Geo-Aware (Ayush et al., 2021) leveraging geo-location information. However, the well-designed handcrafted data structure is a double-edged sword that limits the capabilities of foundation models to some extent. Besides, remote sensing image pairs are sensitive to significant changes in the temporal span, such as major urban development (Mall et al., 2023), natural disasters, and the external environment. Hence, CtxMIM designs a novel MIM framework by taking the natural advantage of abundant remote sensing images captured by sensors daily, making the foundation model easily extended to a larger scale in further research.

Exploring more effective SSL paradigm. Self-supervised learning (SSL) has exhibited remarkable performance in remote sensing analysis. However, SSL in remote sensing lags behind natural images, primarily due to the object density gap between the two domains. As illustrated in Figure 3, natural images, captured in daily scenes, typically feature apparent foreground objects against a relatively simple background. In contrast, remote sensing images, acquired by sensors on satellites, encompass multiple objects within vast and complex scenes, especially no apparent foreground objects. Due to the enormous object density gap, advanced SSL methods in remote sensing still suffer from **3M** problem: (1) **M**ismatched positive pairs augmented from one remote sensing image; (2) **M**issing contextual information caused by random masking strategies; (3) **M**echanism in pretraining dataset collection. We rethink: *is SSL paradigm effective for remote sensing representation learning?* We explore this answer from the characteristics of remote sensing data and tasks. Since most remote sensing tasks are dense predictions at the object or pixel levels, contrastive method learning representations from two augmented views is less optimal for remote sensing analysis. Our CtxMIM leverages the original image patches masked in MIM to learn good representations from extensive remote sensing images and has illustrated its performance on various tasks.

Limitations and future work. Although CtxMIM is a simple yet powerful MIM method for remote sensing pretraining, we argue that collabo-

rative learning by combining contrastive and reconstructive learning can yield robust representations for remote sensing analysis.

In future work, we will explore a new paradigm of collaborative learning, design a more efficient mask strategy, and employ patch pairs of masked and original to jointly embed contrastive learning into reconstructive learning. With the simple pipeline and the solid performance, we hope this work will inspire other works, not just in the remote sensing community but also in the industry and medical image analysis community.

6. Conclusion

This paper presents CtxMIM, a simple yet efficient masked image modeling for remote sensing representation learning. CtxMIM is built on the insight that the high object density in remote sensing images significantly impedes semantic reasoning for reconstructive learning due to missing contextual information. Therefore, CtxMIM utilizes the original patches and introduces a context-enhanced generative branch, which can provide contextual information through the context consistency constraint. Finally, we train CtxMIM by collecting a large-scale unlabeled remote sensing dataset with 1.28 million images covering rich topography and terrain. Comprehensive experiments on land cover classification, semantic segmentation, object detection, and instance segmentation demonstrate that CtxMIM learns good features with high generalization and transferable ability, significantly outperforming supervised and self-supervised methods.

References

- Assran, M., Caron, M., Misra, I., Bojanowski, P., Bordes, F., Vincent, P., Joulin, A., Rabbat, M., Ballas, N., 2022. Masked siamese networks for label-efficient learning, in: ECCV, pp. 456–473.
- Ayush, K., UzKent, B., Meng, C., Tanmay, K., Burke, M., Lobell, D., Ermon, S., 2021. Geography-aware self-supervised learning, in: ICCV, pp. 10181–10190.
- Bachmann, R., Mizrahi, D., Atanov, A., Zamir, A., 2022. MultimaE: Multi-modal multi-task masked autoencoders, in: ECCV, pp. 348–367.
- Bai, L., Huang, W., Zhang, X., Du, S., Cong, G., Wang, H., Liu, B., 2023. Geographic mapping with unsupervised multi-modal representation learning from vhr images and pois. ISPRS Journal of Photogrammetry and Remote Sensing 201, 193–208.
- Bao, H., Dong, L., Piao, S., Wei, F., 2021. Beit: Bert pre-training of image transformers. arXiv preprint arXiv:2106.08254 .

- Bastani, F., Wolters, P., Gupta, R., Ferdinando, J., Kembhavi, A., 2023. Satlaspretrain: A large-scale dataset for remote sensing image understanding, in: ICCV, pp. 16772–16782.
- Caron, M., Misra, I., Mairal, J., Goyal, P., Bojanowski, P., Joulin, A., 2020. Unsupervised learning of visual features by contrasting cluster assignments, in: NeurIPS, pp. 9912–9924.
- Chen, H., Song, J., Wu, C., Du, B., Yokoya, N., 2023. Exchange means change: An unsupervised single-temporal change detection framework based on intra-and inter-image patch exchange. *ISPRS Journal of Photogrammetry and Remote Sensing* 206, 87–105.
- Chen, T., Kornblith, S., Norouzi, M., Hinton, G., 2020a. A simple framework for contrastive learning of visual representations, in: ICML, pp. 1597–1607.
- Chen, X., Fan, H., Girshick, R., He, K., 2020b. Improved baselines with momentum contrastive learning. *arXiv preprint arXiv:2003.04297*.
- Chen, X., He, K., 2021. Exploring simple siamese representation learning, in: CVPR, pp. 15750–15758.
- Cheng, G., Han, J., Lu, X., 2017. Remote sensing image scene classification: Benchmark and state of the art. *Proceedings of the IEEE* 105, 1865–1883.
- Christie, G., Fendley, N., Wilson, J., Mukherjee, R., 2018. Functional map of the world, in: CVPR, pp. 6172–6180.
- Cong, Y., Khanna, S., Meng, C., Liu, P., Rozi, E., He, Y., Burke, M., Lobell, D., Ermon, S., 2022. Satmae: Pre-training transformers for temporal and multi-spectral satellite imagery, in: NeurIPS, pp. 197–211.
- Dosovitskiy, A., Beyer, L., Kolesnikov, A., Weissenborn, D., Zhai, X., Unterthiner, T., Dehghani, M., Minderer, M., Heigold, G., Gelly, S., et al., 2020. An image is worth 16x16 words: Transformers for image recognition at scale, in: ICLR.
- Drusch, M., Del Bello, U., Carlier, S., Colin, O., Fernandez, V., Gascon, F., Hoersch, B., Isola, C., Laberinti, P., Martimort, P., et al., 2012. Sentinel-2: Esa’s optical high-resolution mission for gmes operational services. *Remote Sens. Environ.* 120, 25–36.
- Fang, B., Chen, G., Kou, R., Paoletti, M.E., Haut, J.M., Plaza, A., 2023. Cit: Content-invariant translation with hybrid attention mechanism for unsupervised change detection. *ISPRS Journal of Photogrammetry and Remote Sensing* 204, 321–339.
- Fang, Y., Dong, L., Bao, H., Wang, X., Wei, F., 2022. Corrupted image modeling for self-supervised visual pre-training. *arXiv preprint arXiv:2202.03382*.
- de Gélis, I., Saha, S., Shahzad, M., Corpetti, T., Lefèvre, S., Zhu, X.X., 2023. Deep unsupervised learning for 3d als point clouds change detection. *ISPRS Open Journal of Photogrammetry and Remote Sensing* 9, 100044.
- Gorelick, N., Hancher, M., Dixon, M., Ilyushchenko, S., Thau, D., Moore, R., 2017. Google earth engine: Planetary-scale geospatial analysis for everyone. *Remote Sens. Environ.* 202, 18–27.
- Grill, J.B., Strub, F., Altché, F., Tallec, C., Richemond, P., Buchatskaya, E., Doersch, C., Avila Pires, B., Guo, Z., Gheshlaghi Azar, M., et al., 2020. Bootstrap your own latent—a new approach to self-supervised learning, in: NeurIPS, pp. 21271–21284.
- Guo, T., Liu, H., Chen, Z., Liu, M., Wang, T., Ding, R., 2022. Contrastive learning from extremely augmented skeleton sequences for self-supervised action recognition, in: AAAI, pp. 762–770.
- Gupta, A., Wu, J., Deng, J., Li, F.F., 2024. Siamese masked autoencoders, in: NeurIPS.
- He, J., Yuan, Q., Li, J., Xiao, Y., Zhang, L., 2023a. A self-supervised remote sensing image fusion framework with dual-stage self-learning and spectral super-resolution injection. *ISPRS Journal of Photogrammetry and Remote Sensing* 204, 131–144.
- He, K., Chen, X., Xie, S., Li, Y., Dollár, P., Girshick, R., 2022a. Masked autoencoders are scalable vision learners, in: CVPR, pp. 16000–16009.
- He, K., Fan, H., Wu, Y., Xie, S., Girshick, R., 2020. Momentum contrast for unsupervised visual representation learning, in: CVPR, pp. 9729–9738.
- He, K., Gkioxari, G., Dollár, P., Girshick, R., 2017. Mask r-cnn, in: ICCV, pp. 2961–2969.
- He, K., Zhang, X., Ren, S., Sun, J., 2016. Deep residual learning for image recognition, in: CVPR, pp. 770–778.
- He, Q., Sun, X., Yan, Z., Wang, B., Zhu, Z., Diao, W., Yang, M.Y., 2023b. Ast: Adaptive self-supervised transformer for optical remote sensing representation. *ISPRS Journal of Photogrammetry and Remote Sensing* 200, 41–54.
- He, S., Li, Q., Liu, Y., Wang, W., 2022b. Semantic segmentation of remote sensing images with self-supervised semantic-aware inpainting. *IEEE Geosci. Remote Sens. Lett.* 19, 1–5.
- Helber, P., Bischke, B., Dengel, A., Borth, D., 2019. Eurosat: A novel dataset and deep learning benchmark for land use and land cover classification. *IEEE J. Sel. Topics Appl. Earth Observ. Remote Sens.* 12, 2217–2226.
- Hong, D., Zhang, B., Li, X., Li, Y., Li, C., Yao, J., Yokoya, N., Li, H., Ghamisi, P., Jia, X., et al., 2024. Spectralgpt: Spectral remote sensing foundation model. *IEEE Trans. Pattern Anal. Mach. Intell.*
- Huang, Z., Zhang, M., Gong, Y., Liu, Q., Wang, Y., 2024. Generic knowledge boosted pre-training for remote sensing images. *IEEE Trans. Geosci. Remote Sens.*
- Jung, H., Oh, Y., Jeong, S., Lee, C., Jeon, T., 2021. Contrastive self-supervised learning with smoothed representation for remote sensing. *IEEE Geosci. Remote Sens. Lett.* 19, 1–5.
- Kang, J., Fernandez-Beltran, R., Duan, P., Liu, S., Plaza, A.J., 2020. Deep unsupervised embedding for remotely sensed images based on spatially augmented momentum contrast. *IEEE Trans. Geosci. Remote Sens.* 59, 2598–2610.
- Kim, D., Song, B.C., 2021. Contrastive adversarial learning for person independent facial emotion recognition, in: AAAI, pp. 5948–5956.
- Lam, D., Kuzma, R., McGee, K., Dooley, S., Laielli, M., Klaric, M., Bulatov, Y., McCord, B., 2018. xview: Objects in context in overhead imagery. *arXiv preprint arXiv:1802.07856*.
- Li, H., Li, Y., Zhang, G., Liu, R., Huang, H., Zhu, Q., Tao, C., 2022a. Global and local contrastive self-supervised learning for semantic segmentation of hr remote sensing images. *IEEE Trans. Geosci. Remote Sens.* 60, 1–14.
- Li, W., Chen, H., Shi, Z., 2021a. Semantic segmentation of remote sensing images with self-supervised multitask representation learning. *IEEE J. Sel. Topics Appl. Earth Observ. Remote Sens.* 14, 6438–6450.
- Li, W., Chen, K., Chen, H., Shi, Z., 2021b. Geographical knowledge-driven representation learning for remote sensing images. *IEEE Trans. Geosci. Remote Sens.* 60, 1–16.
- Li, W., Chen, K., Shi, Z., 2022b. Geographical supervi-

- sion correction for remote sensing representation learning. *IEEE Trans. Geosci. Remote Sens.* 60, 1–20.
- Li, Y., Hu, P., Liu, Z., Peng, D., Zhou, J.T., Peng, X., 2021c. Contrastive clustering, in: *AAAI*, pp. 8547–8555.
- Lin, T.Y., Goyal, P., Girshick, R., He, K., Dollár, P., 2017. Focal loss for dense object detection, in: *ICCV*, pp. 2980–2988.
- Lin, T.Y., Maire, M., Belongie, S., Hays, J., Perona, P., Ramanan, D., Dollár, P., Zitnick, C.L., 2014. Microsoft coco: Common objects in context, in: *ECCV*, Springer. pp. 740–755.
- Liu, J., Huang, X., Zheng, J., Liu, Y., Li, H., 2023a. Mixmae: Mixed and masked autoencoder for efficient pretraining of hierarchical vision transformers, in: *CVPR*, pp. 6252–6261.
- Liu, Z., Gui, J., Luo, H., 2023b. Good helper is around you: Attention-driven masked image modeling, in: *AAAI*, pp. 1799–1807.
- Liu, Z., Lin, Y., Cao, Y., Hu, H., Wei, Y., Zhang, Z., Lin, S., Guo, B., 2021. Swin transformer: Hierarchical vision transformer using shifted windows, in: *ICCV*, pp. 10012–10022.
- Long, Y., Xia, G.S., Li, S., Yang, W., Yang, M.Y., Zhu, X.X., Zhang, L., Li, D., 2021. On creating benchmark dataset for aerial image interpretation: Reviews, guidelines, and million-aid. *IEEE J. Sel. Topics Appl. Earth Observ. Remote Sens.* 14, 4205–4230.
- Mall, U., Hariharan, B., Bala, K., 2023. Change-aware sampling and contrastive learning for satellite images, in: *CVPR*, pp. 5261–5270.
- Manas, O., Lacoste, A., Giró-i Nieto, X., Vazquez, D., Rodriguez, P., 2021. Seasonal contrast: Unsupervised pre-training from uncurated remote sensing data, in: *ICCV*, pp. 9414–9423.
- Mendieta, M., Han, B., Shi, X., Zhu, Y., Chen, C., 2023. Towards geospatial foundation models via continual pre-training, in: *ICCV*, pp. 16806–16816.
- Muhtar, D., Zhang, X., Xiao, P., 2022. Index your position: A novel self-supervised learning method for remote sensing images semantic segmentation. *IEEE Trans. Geosci. Remote Sens.* 60, 1–11.
- Muhtar, D., Zhang, X., Xiao, P., Li, Z., Gu, F., 2023. Cmid: A unified self-supervised learning framework for remote sensing image understanding. *IEEE Trans. Geosci. Remote Sens.* .
- Noman, M., Naseer, M., Cholakkal, H., Anwar, R.M., Khan, S., Khan, F.S., 2024. Rethinking transformers pre-training for multi-spectral satellite imagery. *arXiv preprint arXiv:2403.05419* .
- Oord, A.v.d., Li, Y., Vinyals, O., 2018. Representation learning with contrastive predictive coding. *arXiv preprint arXiv:1807.03748* .
- Reed, C.J., Gupta, R., Li, S., Brockman, S., Funk, C., Clipp, B., Keutzer, K., Candido, S., Uyttendaele, M., Darrell, T., 2023. Scale-mae: A scale-aware masked autoencoder for multiscale geospatial representation learning, in: *ICCV*, pp. 4088–4099.
- Reiss, T., Hoshen, Y., 2023. Mean-shifted contrastive loss for anomaly detection, in: *AAAI*, pp. 2155–2162.
- Russakovsky, O., Deng, J., Su, H., Krause, J., Satheesh, S., Ma, S., Huang, Z., Karpathy, A., Khosla, A., Bernstein, M., et al., 2015. Imagenet large scale visual recognition challenge. *Int. J. Comput. Vis.* 115, 211–252.
- Scheibenreif, L., Hanna, J., Mommert, M., Borth, D., 2022. Self-supervised vision transformers for land-cover segmentation and classification, in: *CVPR*, pp. 1422–1431.
- Stojnic, V., Risojevic, V., 2021. Self-supervised learning of remote sensing scene representations using contrastive multiview coding, in: *CVPR*, pp. 1182–1191.
- Sun, W., Li, J., Jiang, M., Yuan, Q., 2023. Supervised and self-supervised learning-based cascade spatiotemporal fusion framework and its application. *ISPRS Journal of Photogrammetry and Remote Sensing* 203, 19–36.
- Tang, M., Cozma, A., Georgiou, K., Qi, H., 2024. Cross-scale mae: A tale of multiscale exploitation in remote sensing, in: *NeurIPS*.
- Tang, M., Georgiou, K., Qi, H., Champion, C., Bosch, M., 2023. Semantic segmentation in aerial imagery using multi-level contrastive learning with local consistency, in: *WACV*, pp. 3798–3807.
- Tao, C., Qi, J., Zhang, G., Zhu, Q., Lu, W., Li, H., 2023. Tov: The original vision model for optical remote sensing image understanding via self-supervised learning. *IEEE J. Sel. Topics Appl. Earth Observ. Remote Sens.* .
- Tian, Y., Krishnan, D., Isola, P., 2020. Contrastive multiview coding, in: *ECCV*, pp. 776–794.
- Tong, Z., Song, Y., Wang, J., Wang, L., 2022. Videomae: Masked autoencoders are data-efficient learners for self-supervised video pre-training, in: *NeurIPS*, pp. 10078–10093.
- Van Etten, A., Lindenbaum, D., Bacastow, T.M., 2018. Spacenet: A remote sensing dataset and challenge series. *arXiv preprint arXiv:1807.01232* .
- Vincenzi, S., Porrello, A., Buzzega, P., Cipriano, M., Fronte, P., Cucu, R., Ippoliti, C., Conte, A., Calderara, S., 2021. The color out of space: learning self-supervised representations for earth observation imagery, in: *ICPR*, pp. 3034–3041.
- Wang, Z., Ng, M.K., Michalski, J., Zhuang, L., 2023. A self-supervised deep denoiser for hyperspectral and multispectral image fusion. *IEEE Trans. Geosci. Remote Sens.* .
- Wei, C., Fan, H., Xie, S., Wu, C.Y., Yuille, A., Feichtenhofer, C., 2022. Masked feature prediction for self-supervised visual pre-training, in: *CVPR*, pp. 14668–14678.
- Xia, G.S., Bai, X., Ding, J., Zhu, Z., Belongie, S., Luo, J., Datcu, M., Pelillo, M., Zhang, L., 2018. Dota: A large-scale dataset for object detection in aerial images, in: *CVPR*, pp. 3974–3983.
- Xie, Z., Zhang, Z., Cao, Y., Lin, Y., Bao, J., Yao, Z., Dai, Q., Hu, H., 2022. Simmim: A simple framework for masked image modeling, in: *CVPR*, pp. 9653–9663.
- Xu, Y., Ma, Y., Zhang, Z., 2024. Self-supervised pre-training for large-scale crop mapping using sentinel-2 time series. *ISPRS Journal of Photogrammetry and Remote Sensing* 207, 312–325.
- Zbontar, J., Jing, L., Misra, I., LeCun, Y., Deny, S., 2021. Barlow twins: Self-supervised learning via redundancy reduction, in: *ICML*, pp. 12310–12320.
- Zeng, Q., Geng, J., 2022. Task-specific contrastive learning for few-shot remote sensing image scene classification. *ISPRS Journal of Photogrammetry and Remote Sensing* 191, 143–154.
- Zhang, X., Zhu, B., Yao, X., Sun, Q., Li, R., Yu, B., 2022. Context-based contrastive learning for scene text recognition, in: *AAAI*, pp. 3353–3361.
- Zhao, H., Zhang, Y., Liu, S., Shi, J., Loy, C.C., Lin, D., Jia, J., 2018. Psanet: Point-wise spatial attention network for scene parsing, in: *ECCV*, pp. 267–283.